The Dynamical Influence of the Atlantic Multidecadal Oscillation on Continental Climate

CHRISTOPHER H. O'REILLY, TIM WOOLLINGS, AND LAURE ZANNA

Atmospheric, Oceanic and Planetary Physics, Department of Physics, University of Oxford, Oxford, United Kingdom

(Manuscript received 28 April 2016, in final form 30 May 2017)

ABSTRACT

The Atlantic multidecadal oscillation (AMO) in sea surface temperature (SST) has been shown to influence the climate of the surrounding continents. However, it is unclear to what extent the observed impact of the AMO is related to the thermodynamical influence of the SST variability or the changes in large-scale atmospheric circulation. Here, an analog method is used to decompose the observed impact of the AMO into dynamical and residual components of surface air temperature (SAT) and precipitation over the adjacent continents. Over Europe the influence of the AMO is clearest during the summer, when the warm SAT anomalies are interpreted to be primarily thermodynamically driven by warm upstream SST anomalies but also amplified by the anomalous atmospheric circulation. The overall precipitation response to the AMO in summer is generally less significant than the SAT but is mostly dynamically driven. The decomposition is also applied to the North American summer and the Sahel rainy season. Both dynamical and residual influences on the anomalous precipitation over the Sahel are substantial, with the former dominating over the western Sahel region and the latter being largest over the eastern Sahel region. The results have potential implications for understanding the spread in AMO variability in coupled climate models and decadal prediction systems.

1. Introduction

North Atlantic sea surface temperature (SST) exhibits low-frequency variability, on the order of multiple decades, which is referred to as Atlantic multidecadal variability or the Atlantic multidecadal oscillation (AMO) (Enfield et al. 2001). Over North America, the warm phase of the AMO is associated with warmer summers and significantly drier conditions over much of the south and southeast of the continent for most of the year (McCabe et al. 2004; Nigam et al. 2011; Ruiz-Barradas and Nigam 2005; Sutton and Hodson 2005), with opposing effects during the cold phase of the AMO. Over Africa, the warm phase of the AMO is associated with a large increase in Sahel precipitation during the rainy season, with drier conditions in the cool phase (Folland et al. 1986; Knight et al. 2006; Martin and Thorncroft 2014b; Ting et al. 2009).

The observed influence of the AMO over Europe depends on the season. During summer, the warm phase of the AMO is associated with warmer surface air temperatures over most of the continent and increased precipitation over northwestern Europe (Knight et al. 2006; Sutton and Dong 2012; Sutton and Hodson 2005). It has also been shown that the AMO influences the length of European summers, which are longer in the warm phase of the AMO (Peña-Ortiz et al. 2015). The autumn is generally associated with warmer temperatures, particularly in northern Europe, during the warm phase of the AMO, whereas the spring is mainly associated with warmer temperatures over western Europe (Sutton and Dong 2012). These regional differences in season are associated with large-scale atmospheric circulation anomalies, such that a substantial portion of the observed anomalies in temperature or precipitation associated with the AMO variability may be due to the anomalous flow patterns rather than

Denotes content that is immediately available upon publication as open access.

Supplemental information related to this paper is available at the Journals Online website: http://dx.doi.org/10.1175/JCLI-D-16-0345.s1.

Corresponding author: Christopher H. O'Reilly, christopher.oreilly@physics.ox.ac.uk

DOI: 10.1175/JCLI-D-16-0345.1

© 2017 American Meteorological Society. For information regarding reuse of this content and general copyright information, consult the AMS Copyright Policy (www.ametsoc.org/PUBSReuseLicenses).

directly associated with warmer conditions upstream over the North Atlantic. This may also be the case during winter, when the warm phase of the AMO has been linked by some studies with cold temperature anomalies over much of central and western Europe (Gastineau and Frankignoul 2015; Häkkinen et al. 2011; Peings and Magnusdottir 2014; Ting et al. 2014; Yamamoto and Palter 2016). However, the extent to which the observed impact on European climate is dependent on the anomalous large-scale circulation response, which also varies by season, remains unclear.

Recently there have been significant efforts to model the impact of AMO variability on the climate of the surrounding continents. This is especially important given the relatively short observational record. The circulation fields exhibit significant variability between model simulations, vary by model, and are also dependent on variability in the tropical Pacific (Schubert et al. 2009) but do manage to capture many of the key features. For example, over Europe, idealized experiments with prescribed SSTs do capture, to some extent, the negative summer NAO response (Folland et al. 2009) to the warm phase of the AMO, with a negative SLP anomaly over the United Kingdom (Msadek et al. 2011; Sutton and Hodson 2005), albeit weaker than in the observations; this has also been seen in simulations using coupled climate models (Knight et al. 2006) and is consistent with a linear baroclinic response to surface heating (Ghosh et al. 2016). The low geopotential anomaly observed downstream of the warm midlatitude North Atlantic SST anomaly during summer has also been demonstrated in a series of aquaplanet experiments by Veres and Hu (2015). In the CMIP5 models, however, the extratropical circulation response to the AMO is poorly captured in all seasons (Kavvada et al. 2013; Peings et al. 2016), although the models are able to somewhat realistically capture the influence of North Atlantic SSTs on the West African monsoon (Martin and Thorncroft 2014a; Ting et al. 2011). As such, the large spread in model response to the AMO in different regions and seasons is likely related to the differing ability with which they are able to capture the observed circulation response.

While model simulations have helped to elucidate how the atmospheric circulation responds to the AMO, to what extent these circulation anomalies govern the impact of the AMO on the surrounding continents is not at all clear. In this paper, we estimate the contribution of the circulation anomalies associated with the AMO to the observed impact of the AMO on surface climate. To do this we employ a constructed circulation analog technique (Deser et al. 2016) to decompose the impact of the AMO on precipitation and surface air temperature. This reveals a dynamical response to the AMO and a residual, which in many cases can be interpreted as a thermodynamic response. The contribution of the circulation anomalies to the observed impact of the AMO is found to vary by season and region. This method sheds light on why models do not tend to perform well in capturing certain features in response to the AMO. The datasets and dynamical circulation analog methods are described in the following section. In section 3, we analyze the decomposed response to the AMO over Europe in the different seasons, focusing mainly on the summer. We then discuss the decomposed response over Africa and North America in section 4. A brief summary and further discussion follows in section 5.

2. Methods

a. Datasets

We analyze data from the period 1901–2010, inclusive, which is the common period of all datasets used in the study. To assess the impact of the AMO over continental regions, we use surface air temperature (SAT) and precipitation over land from the Climatic Research Unit Time Series (CRU TS), version 3.23 (Harris et al. 2014), on a 0.5° × 0.5° grid. We use SSTs from the Hadley Centre Sea Ice and Sea Surface Temperature dataset (HadISST; Rayner et al. 2003) on a 1° × 1° grid.

Dynamical circulation analogs (described below) were produced using monthly mean sea level pressure (SLP) anomalies from three different datasets. Multiple SLP datasets are considered because together they can provide a measure of the robustness (and to an extent the uncertainty) of the atmospheric circulation anomalies, and the relevant dynamical decomposition, associated with the AMO. The first is the European Centre for Medium-Range Weather Forecasts twentieth century reanalysis (ERA-20C) dataset (Poli et al. 2013), on a 2.5° × 2.5° grid, which is produced by assimilating only surface pressure and marine wind observations. The second SLP dataset is the Twentieth Century Reanalysis (20CR) (Compo et al. 2011), on a 2° × 2° grid, which is also an atmospheric reanalysis that is produced by assimilating surface pressure and marine wind observations. The final SLP dataset analyzed is the second Hadley Centre Sea Level Pressure dataset (HadSLP2) (Allan and Ansell 2006), on a coarser 5° × 5° grid, which is produced from marine observations and station observations over land with missing data filled using an optimal interpolation method. We will present results from ERA-20C, but differences and similarities with respect to 20CR and HadSLP2 will be discussed (and some additional plots for 20CR and HadSLP2 are also included in the supplemental material).

For all datasets, monthly mean anomalies were calculated by removing a monthly climatology from monthly averaged data over the period of our analysis, from January 1901 to December 2010. The anomalies were then linearly detrended over the whole period. The results presented in this paper were also tested with a quadratic detrending, and the qualitative findings were not found to be sensitive to the method of detrending (see Fig. S13 in the supplemental material for an example).

b. *Constructed circulation analogs*

To estimate the components of precipitation and SAT that are solely due to atmospheric circulation anomalies, we compute empirical circulation analogs, applying the constructed circulation analog method of Deser et al. (2016). Analog techniques have previously been used for statistical weather forecasting (Lorenz 1969; Van den Dool 1994; Van den Dool et al. 2003) and, more recently, to assess the role of global warming on cold European winters (Cattiaux et al. 2010). The constructed analog method used here aims to calculate the SAT (or precipitation) anomalies that are associated with the large-scale circulation anomalies and is similar to the gridpoint partial least squares method employed by Smoliak et al. (2010), Wallace et al. (2012), and Smoliak et al. (2015). The Deser et al. (2016) method is preferred here because the calculation that produces the circulation analogs can be simply extended to other fields, to construct the anomaly associated with a particular circulation pattern. Deser et al. (2016) demonstrated (in Fig. S1 of their paper) that the constructed approach yields similar estimates as the pointwise partial least squares method of Smoliak et al. (2015) for the dynamical contribution to observed wintertime SAT trends over North America.

We use monthly SLP anomalies to characterize the dynamical circulation anomalies. For each month, the Euclidean distance is calculated between the (area weighted) SLP anomaly of the target month and all other SLP anomalies corresponding to the same calendar month (i.e., each January is compared with all other Januaries). The Euclidean distance is calculated on the target region: for example, the European region is defined as 30°–90°N, 60°W–60°E. The 80 months that are closest to the target month are then selected, excluding those that occur within 5 years of the target month to avoid sampling the neighboring years. A subsample of 50 months is then randomly selected from the set of the 80 closest months. We then calculate the optimal linear fit (in a least squares sense) of the 50-month subsample to the target SLP field, using multiple linear regression. Fitting this subsample of 50 months to the target month yields a regression coefficient for each of the 50 months, which can be used to construct the analog SLP anomaly. The random subsampling and fitting to the target SLP field is repeated 100 times, and the resulting 100 constructed SLP fields are then averaged to obtain an analog SLP field. The repeated subsampling ensures that the analog SLP field closely represents the target SLP field but is not overly determined by any particular month in the dataset. We found the results are insensitive to the exact number of ''closest'' months, number of subsampled months, or the number of repeated subsamples performed [see also the appendix of Deser et al. (2016)].

The dynamical SAT and precipitation analog fields, associated with the circulation anomaly, are calculated during the procedure that calculates the analog SLP field. When calculating the optimal linear fit to the target SLP field, the regression coefficients yielded are multiplied by the SAT/precipitation anomaly for the respective month. The subsampling results in 100 estimates for the dynamical SAT/precipitation anomaly, which are averaged to obtain a ''best'' estimate of the dynamical SAT/precipitation anomaly. This process is repeated for every month in the SAT and precipitation datasets. The monthly full and dynamical anomalies for each field are averaged over 3-month periods to produce seasonal anomalies; the residual anomaly is then calculated by subtracting the dynamical anomaly from the full anomaly. In section 3a, we estimate the uncertainty in this by using the 100 random subsamples used to produce the constructed analogs for each month. One of the subsamples for each month in a season is randomly selected, and these are combined to produce one seasonal analog. This process is then repeated 1000 times, and the uncertainty is measured from the resulting distribution.

To estimate the uncertainty in the dynamical decomposition, the 100 random subsamples used to produce the constructed analogs for each month were randomly combined 1000 times, producing 1000 random seasonal analogs (the shading in Fig. 7, described in greater detail below, indicates the 5%–95% range of this distribution for each year).

An example of the dynamical circulation analog over Europe for the summer season [defined as the June–August mean (JJA)] is shown in Fig. 1 for the year 1990. The full SLP anomaly for the season is clearly well captured throughout the European sector by the dynamical SLP anomaly field (cf. Fig. 1a with Fig. 1b), which was constructed using the analog technique. The residual SLP anomaly is small everywhere within the European target region, which gives confidence that the analog method is able to effectively reconstruct the seasonal circulation anomalies. The year 1990 is selected at random, but the

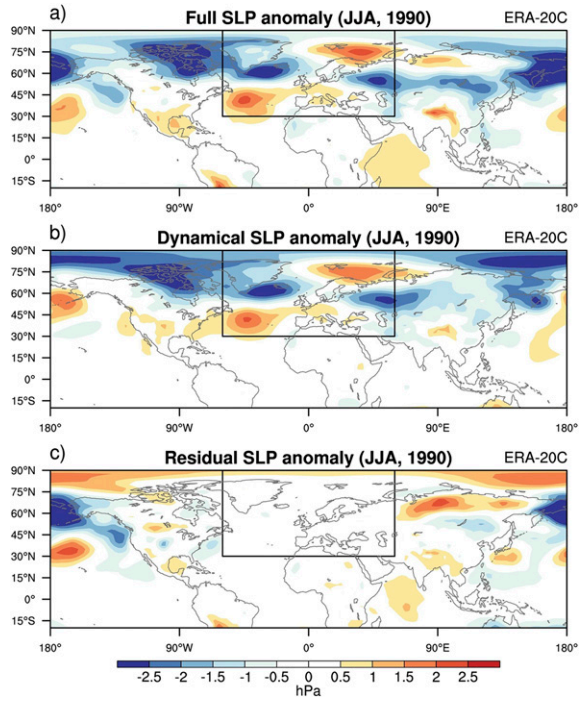

FIG. 1. Example of the dynamical analog SLP reconstruction for summer (i.e., JJA) of 1990 for (a) the full SLP anomaly, (b) the dynamical SLP anomaly produced using the analog reconstruction method, and (c) the residual SLP anomaly.

scales of the seasonal SLP anomalies over the European sector are not particularly unusual, and the residual is similarly small for all seasons and years. To test how well the constructed analog SLP anomalies are able to capture the full anomaly fields for each season, we calculated the fraction of the explained variance (i.e., the squared correlation coefficient r^2) for each season, and almost 100% of the variance of the full SLP anomaly fields is captured by the constructed analogs in all seasons (see Fig. S1 for an example for the European winter analogs).

The decomposition of SAT and precipitation anomalies for summer 1990 are shown in Fig. 2. For this particular season, the dynamical circulation analogs suggest that the cold anomaly over eastern Europe (Fig. 2a) is primarily dynamically induced by northerly winds associated with the western edge of the cyclonic circulation anomaly. Over Scandinavia the temperature anomalies are weak, given what would be estimated using this method from the anomalous circulation alone [i.e., the dynamical SAT anomaly (Fig. 2c)], which would typically be associated with warm anomalies as a result of anomalous southerly flow. The residual SAT anomaly is therefore cold over Scandinavia. The largest residual SAT anomaly is found over northern Russia, on the eastern edge of the analysis region. While this may be related to SLP anomalies from outside the region of interest, maps of the fraction of explained variance (shown later in Fig. 3) do not show an abrupt drop close to the edge of the analysis region; for example, the explained variance fraction drops to 0.5 about 10° outside the target region (i.e., Fig. S1). The decomposition of precipitation is less clear, largely because of the smaller scale of the precipitation anomalies themselves. The dry anomaly over central and western Europe occurs under a region of anomalous high pressure, whereas the positive precipitation anomaly over Russia occurs under a region of anomalous low pressure. This dynamical precipitation anomaly broadly corresponds to the full precipitation anomaly (i.e., Fig. 2b), but there is still a sizeable residual precipitation anomaly (i.e., Fig. 2f), particularly around the Black Sea, where the dry anomalies are not captured by the dynamical precipitation.

From the dynamical anomaly fields calculated for each year and each season, we can analyze how much of the total interannual variability for each field can be explained by the dynamically induced anomalies. The fraction of variance explained (i.e., r^2) by the dynamical anomaly fields over Europe for each season is shown in Fig. 3. In terms of SAT variability, the dynamical anomalies explain the majority of the variability over the entire continent during winter [December–February (DJF)], whereas, in the other seasons, the dynamical component accounts for around 50% of the variance over most of the continent. The fraction of total interannual precipitation variability that is explained by the dynamical anomalies is much noisier than the equivalent SAT fields, which is likely because of the shorter length scale of precipitation anomalies compared to SAT anomalies. During all seasons, the highest fraction of variance explained by the dynamical component occurs over northwestern Europe and is particularly striking in winter (i.e., Fig. 3b). Farther downstream, over eastern Europe and Russia, there is more spread between the different seasons.

The residual anomaly in each dataset will include any influences from thermodynamic processes: for example, the advection by the climatological flow of the anomalous air temperature and humidity over the ocean, local radiative forcing from clouds, and soil moisture anomalies, which are not directly linked to circulation anomalies. Of course, the residual anomalies are also likely to include a reasonable amount of ''noise'' that is not clearly related to thermodynamics but results from the empirical nature of the decomposition. However, we anticipate that much of this noise will be filtered out when calculating composite differences of the anomaly fields between the warm and cold phases of the AMO

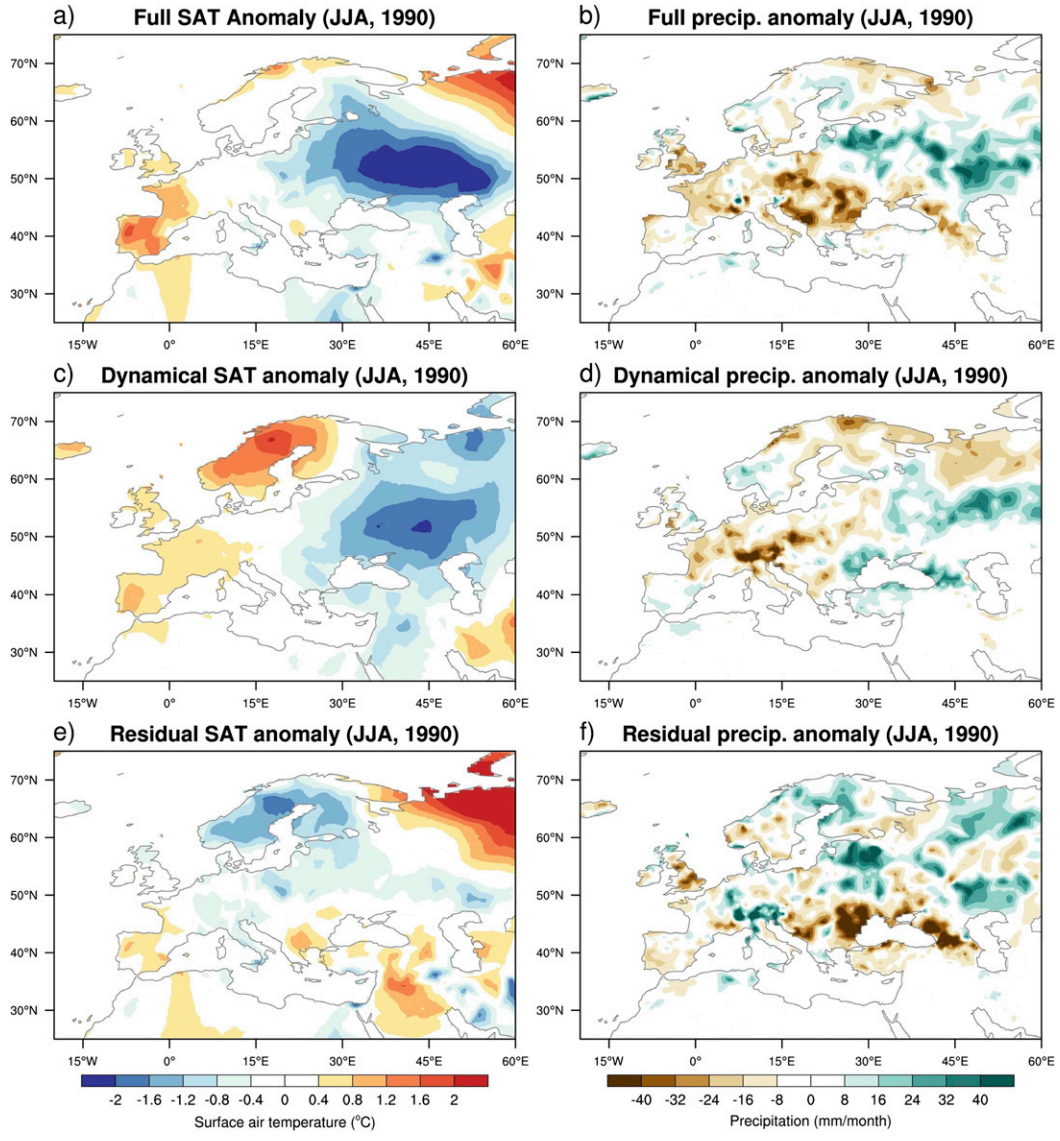

FIG. 2. Example of the dynamical analogs for (left) SAT and (right) precipitation associated with the circulation anomalies for summer (i.e., JJA) of 1990 for (a),(b) the full anomalies; (c),(d) the dynamical anomalies produced using the analog reconstruction method; and (e),(f) the residual anomalies.

(section 2c), which is the main focus of this paper. It should be noted that, since we use monthly anomaly data, the impact of smaller-scale dynamical features that occur on time scales less than a month will only be represented if it has a signature in the monthly SLP anomalies. This means that the impact of individual extratropical storms are to some extent expected to be accounted for where the seasonal SLP anomalies are closely related to seasonal storm-track anomalies, which is the case, for example, over Europe during the summer season (Dong et al. 2013). Whereas, smaller mesoscale and convective systems are likely to be represented to some extent in the residual.

c. *AMO index*

To assess the influence of the AMO on the surrounding continental regions, we use an annual AMO index over the North Atlantic region (0°–60°N, 80°–0°W) calculated using linearly detrended[1] SST anomalies, shown in Fig. 4. We use the AMO index to identify warm periods (1931–60 and 1996–2010) and cold periods

[1] The results presented here are not particularly sensitive to the method of detrending (for an example of the European summer, see Fig. S13).

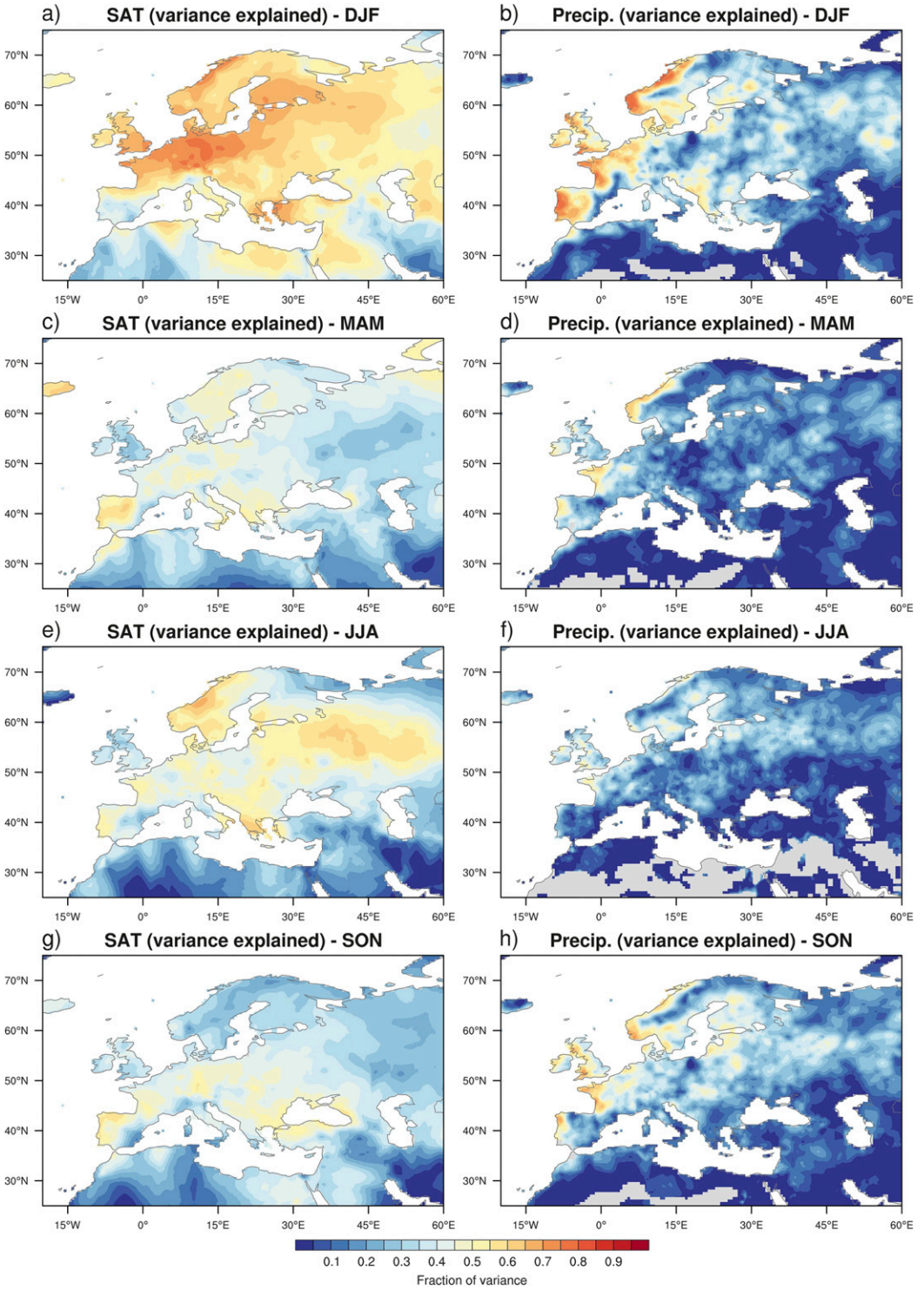

FIG. 3. The fraction of variance explained by the dynamical SAT and precipitation anomalies for each season.

(1902–25 and 1964–93) of the AMO, and these are indicated in Fig. 4. The influence of the AMO on different fields is then estimated by taking composite differences between warm periods and cold periods of the AMO. The same approach was used by Sutton and Dong (2012), and we analyze the same periods; however, Sutton and Dong (2012) only considered the later cold period in their analysis. The differences in SST

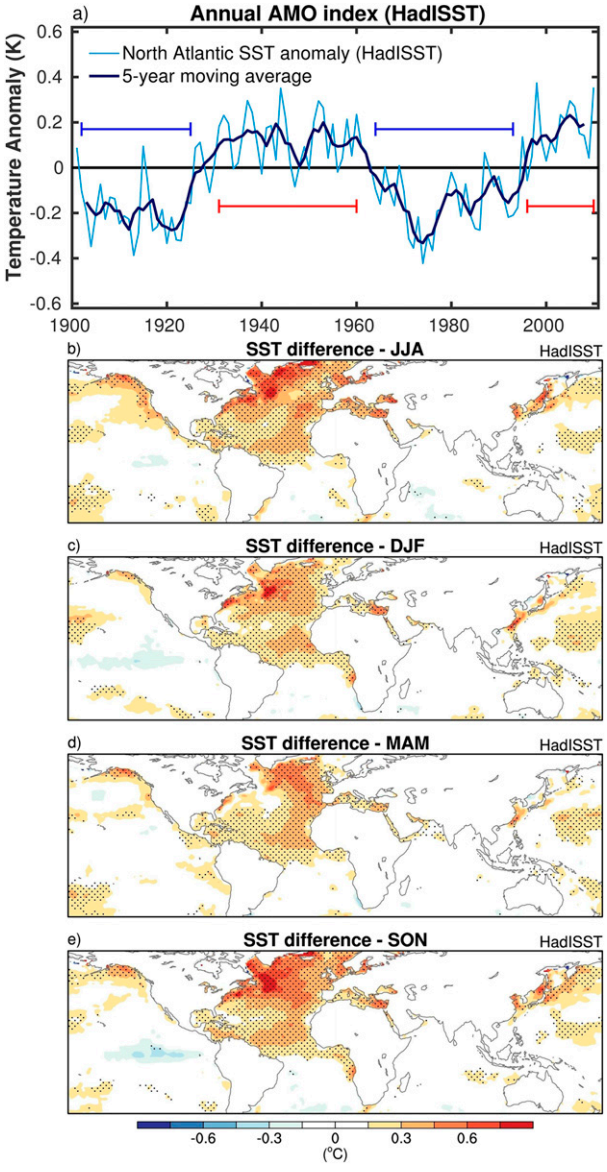

FIG. 4. (a) The time series of the annually averaged detrended SST anomaly averaged over the North Atlantic (0°–60°N, 80°–0°W) is shown in light blue. The 5-yr moving average of the index is overlaid in dark blue. The blue/red horizontal lines indicate the warm periods (1931–60 and 1996–2010) and cold periods (1902–25 and 1964–93) of the AMO. (b)–(e) The difference between (detrended) SST anomalies between warm and cold phases of the AMO. Stippling indicates where the anomalies are significant at the 95% level.

anomalies between the warm and cold periods of the AMO are shown for each season in Fig. 4.

d. Significance tests

The statistical significance of the composite differences between the warm and cold phases of the AMO were calculated using a two-sided Student's *t* test on the seasonally averaged anomalies (e.g., von Storch and Zwiers 2002). The sample size N is taken to be the number of years that make up the warm/cold AMO composites. To account for the year-to-year autocorrelation, the effective sample size was calculated according to $N_{\text{eff}} = N[(1 - r)/(1 + r)]$ (e.g., Bretherton et al. 1999), where N_{eff} is the effective sample size, and r is the lag-1 autocorrelation, calculated at each grid point for each of the different datasets. Negative autocorrelations were set to zero (i.e., $r \geq 0$) such that the effective sample size was never greater than the actual number of years within each composite (i.e., $N_{\text{eff}} \leq N$).

TABLE 1. Spatial correlation values of the dynamical components of the AMO impact [i.e., the dynamical difference maps (e.g., Figs. 6c,d)] for the decomposition calculated using 20CR or HadSLP2, compared with ERA-20C. Values are calculated for the regions shown in the maps of each region, using each grid point over land.

	SAT		Precipitation	
	20CR	HadSLP2	20CR	HadSLP2
Europe in JJA	0.91	0.82	0.71	0.73
Europe in DJF	0.94	0.88	0.71	0.71
Europe in MAM	0.93	0.85	0.75	0.74
Europe in SON	0.72	0.61	0.66	0.49
North America in JJA	0.70	0.68	0.55	0.50
Africa in JJASO	0.92	0.87	0.84	0.68

3. Decomposition of the AMO influence on Europe

We calculate the typical seasonal anomalies associated with the AMO variability by calculating the composite difference between the warm and cold phases of the AMO index (shown in Fig. 4). This is performed for the full, dynamical, and residual seasonal anomalies of SAT and precipitation, as well as SLP. Composite difference maps will be shown for the decomposition using the ERA-20C dataset, but comparisons with the other datasets will be discussed. Pattern correlation of the dynamical SAT/precipitation difference in the ERA-20C dataset with the equivalent 20CR and HadSLP2 composite difference maps are given in Table 1 (the full maps are included in the supplemental material). Where the difference maps of the residual anomaly fields are significant and the decomposition is similar across the different datasets, we can tentatively interpret them as being of thermodynamic origin, an estimate of the anomaly associated with the AMO in the absence of circulation changes. This decomposition allows us to estimate to what extent the observed impact of the

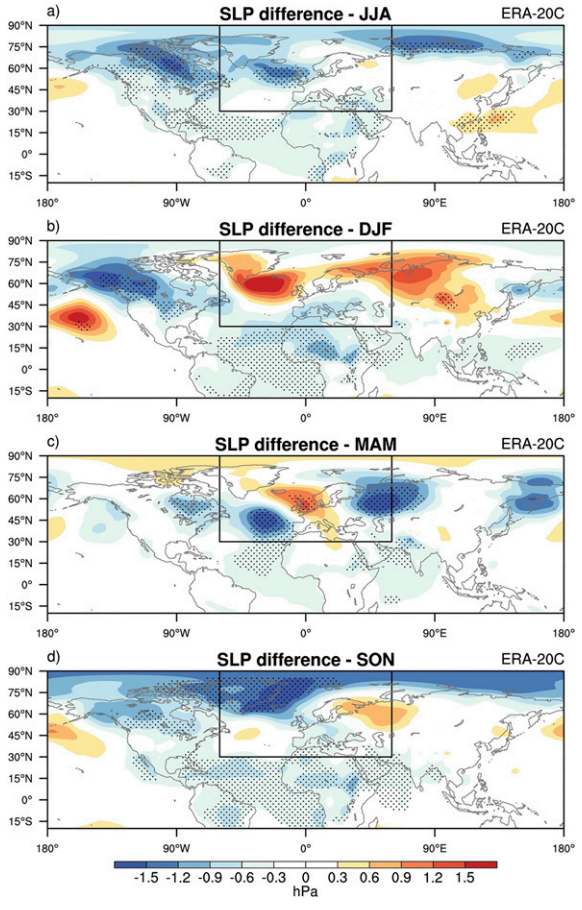

FIG. 5. Seasonal SLP anomaly difference between warm and cold periods of the AMO (as shown in Fig. 4) for (a) JJA, (b) DJF, (c) MAM, and (d) SON. SLP data are from the ERA-20C dataset. Stippling indicates where the SLP anomaly difference is significant at the 95% level.

AMO is as a result of the seasonal circulation anomalies associated with the AMO compared to that which is directly associated with the multidecadal warming/cooling of North Atlantic SST for climatological large-scale circulation conditions. We first analyze the influence of the AMO over Europe.

a. Summer

The warm phase of the AMO in summer (i.e., JJA) generates a cyclonic anomaly over western Europe (Fig. 5a), which is similar to the southern lobe of the negative summer North Atlantic Oscillation (NAO) pattern, as highlighted in previous studies (Ghosh et al. 2016; Sutton and Hodson 2005; Ting et al. 2014). A similar cyclonic anomaly is also found in the 20CR and HadSLP2 datasets (Figs. S2, S3), albeit slightly weaker in the latter. As a result, the composite difference maps of the decomposed anomalies are very similar in all datasets. The difference of the full and decomposed SAT and precipitation anomalies between the warm and cold phases of the AMO for the European summer are shown in Fig. 6. The full SAT anomaly linked to the warm phase of the AMO is similar to that found in previous studies (Knight et al. 2006; Sutton and Dong 2012; Sutton and Hodson 2005), with significant warm anomalies from western Europe to about 45°E (Fig. 6a). However, since these are decadal anomalies, they are still fairly small compared to interannual variability. The largest warm anomalies occur around the Mediterranean. A significant portion of the warm SAT anomalies across Europe is related to the dynamical circulation, as shown by the dynamical SAT anomaly plot (Fig. 6c), but a larger portion is associated with the residual SAT anomaly, apart from over Scandinavia (Fig. 6e). Interestingly, the dynamical and residual anomaly patterns are similar over much of southern Europe, such that the circulation field acts to amplify the warming during the positive phase of the AMO. However, the residual SAT anomaly across southern Europe could be related to the thermodynamic impact of Mediterranean SST anomalies, which are anomalously warm during the warm phase of the AMO, particularly during summer and autumn (Fig. 5).

The influence of the AMO on summertime precipitation over Europe differs from the SAT in that the dynamical anomaly appears to have a dominant influence compared to the residual anomaly (Fig. 6). This is consistent with the larger fraction of variance (i.e., Fig. 3) explained by the dynamical anomaly compared with SAT. The cyclonic anomaly over northwestern Europe (i.e., Fig. 5a) is similar to the southern lobe of the negative summer NAO pattern and is thus associated with more storms and precipitation across northwestern Europe (Bladé et al. 2012; Folland et al. 2009). The dynamical anomaly is responsible for the large-scale features seen in the full anomaly field, with wetter conditions over the northwest of Europe and drier conditions over the southeast of Europe, during the warm phase of the AMO. The residual response does systematically mediate the dynamical anomalies somewhat over the Alps and over eastern Europe, however, where positive residual anomalies act to reduce the dry dynamical anomalies in all datasets.

The dynamical anomalies appear to dominate the response of the precipitation to the AMO more strongly than the SAT, particularly over northwestern Europe. This is also consistent with the impact of the summer NAO, which exhibits a stronger influence on European precipitation anomalies than on SAT anomalies (Bladé et al. 2012). To further investigate the control of the circulation on the SAT and precipitation anomalies over

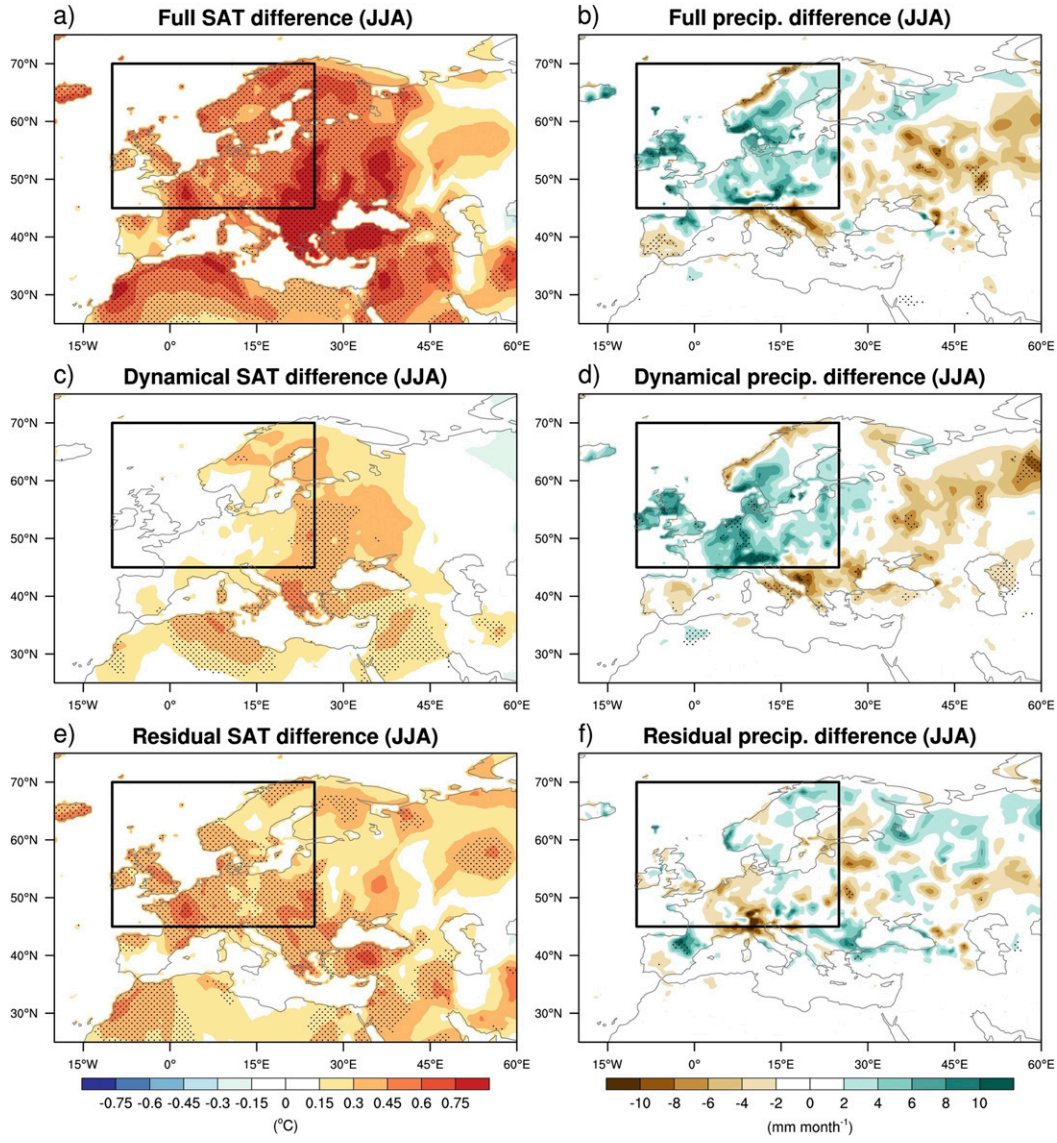

FIG. 6. Summer (JJA) anomaly differences between warm and cold periods of the AMO index for the (a) full SAT anomaly, (c) dynamical SAT anomaly, (e) thermodynamical SAT anomaly, (b) full precipitation anomaly, (d) dynamical precipitation anomaly, and (f) thermodynamical precipitation anomaly. The decomposition was calculated using the ERA-20C. Stippling indicates where the anomalies are significant at the 95% level. The black boxes indicate the northwestern Europe region used to produce the time series in Fig. 7.

the northwestern Europe region, we now analyze indices of the SAT and precipitation averaged over the region (shown in Fig. 6), which are plotted in Fig. 7. Also plotted are the 5-yr averaged SAT and precipitation anomalies as well as the annual and 5-yr AMO indices; the correlation of the SAT and precipitation indices with the respective AMO indices is shown in each panel. A measure of the uncertainty in the decomposition is shown in shading for the annual time series and in bold vertical lines for the 5-yr time series. The uncertainty in the decomposition is relatively small compared to the signal, and it is clear that there is a systematic multidecadal variability in the residual SAT anomaly. Over northwestern Europe there are significant correlations between the annual AMO index and annual SAT ($r = 0.32$, significant at the 95% level), and between the 5-yr AMO index and 5-yr SAT ($r = 0.57$, significant at the 95% level), shown in Fig. 7a. Analysis of the decomposed anomaly indices reveals that the SAT response is dominated by the residual component, which is significantly correlated with the AMO on the annual time scale and particularly on the longer time scale (Fig. 7e)

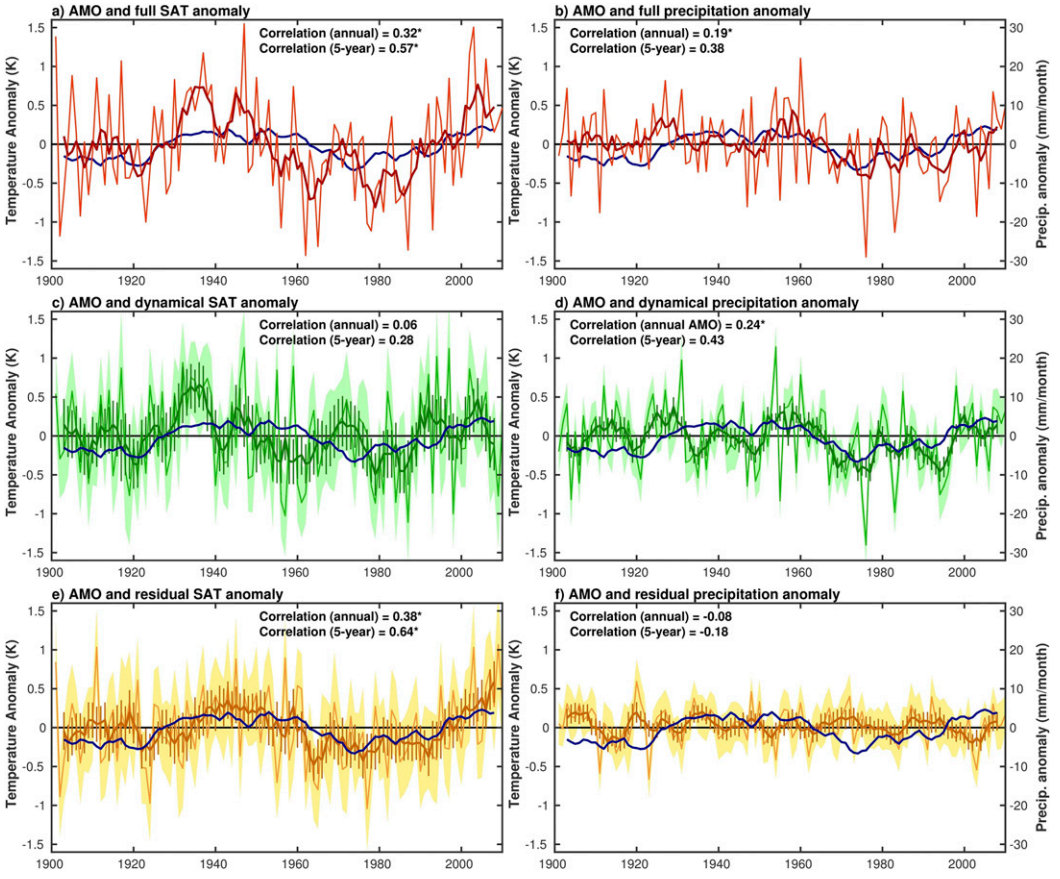

FIG. 7. Annual and 5-yr averaged time series of the summer (i.e., JJA) SAT and precipitation averaged over the northwestern European region (shown in Fig. 6) for the (a) full SAT anomaly, (b) full precipitation anomaly, (c) dynamical SAT anomaly, (d) dynamical precipitation anomaly, (e) thermodynamical SAT anomaly, and (f) thermodynamical precipitation anomaly. The annual indices are in lighter colors, and the 5-yr indices are overlaid in darker colors. The 5%–95% confidence intervals of the random subsampling used to construct dynamical analogs for each year are shown in shading for the annual indices and by vertical lines for the 5-yr indices. The 5-yr AMO index (thick dark blue line, also shown in Fig. 4) is shown for reference. The correlation between each index and the equivalent AMO index is also shown, where an asterisk indicates the correlation is significant at the 95% level, taking into account the effective number of degrees of freedom [using Eq. (31) from Bretherton et al. (1999)].

on which the AMO accounts for over 40% of the variance (i.e., $r = 0.64$, $r^2 = 0.41$). This is consistent with the thermodynamic influence of the advection of warmer air from over the anomalously warm North Atlantic by the climatological summer westerlies, which flow directly over the northwestern Europe region [for climatologies, see, e.g., the ''ERA-40 atlas'' (Kållberg et al. 2005)].

The summer precipitation response to the AMO over northwestern Europe, however, is dominated by the dynamical component (Figs. 7b,d). The AMO exhibits less control on the precipitation though, as none of the components are significantly correlated with the 5-yr index (although in the second half of the time series there is a reasonable relationship). The dynamical index is particularly well correlated with the annual AMO index, but it is difficult to confidently assign a causal response to the annual AMO index because on interannual time scales extratropical SST anomalies (and a significant fraction of the AMO) are primarily forced by atmospheric circulation anomalies (Deser et al. 2010; Gulev et al. 2013). Nonetheless, these results do lend support to the notion that circulation anomalies exhibit a dominant role on the influence of the AMO on summertime precipitation, in comparison with the residual anomaly, particularly over northwestern Europe.

b. *Other seasons*

The decomposition of the AMO influence over Europe was also performed for the autumn, winter, and spring seasons. However, the results do not seem to be particularly robust or as clear as in summer, for several reasons, which we will outline here (Figs. S4–S6 show

example decomposition maps, using the ERA-20C data). In spring, the composite AMO difference consists of significant warm anomalies over much of western Europe and cold anomalies over eastern Europe (Fig. S4). These anomalies are associated with significant large-scale circulation anomalies, consisting of a cyclonic anomaly over the eastern North Atlantic and an anticyclonic anomaly over northern Europe, which is similar in all datasets (Figs. 5b, S2b, and S3b). The decomposition—in all three datasets—reveals that the temperature anomalies are almost entirely as a result of the large-scale circulation anomalies, unlike in summer, with comparably weak residual SAT anomalies (Fig. S4).

During autumn, while the AMO is clearly associated with warm SAT and positive precipitation anomalies over western Europe, the decomposition is less clear than in the summer. The three SLP datasets exhibit little similarity in the SLP anomalies (Figs. 5d, S2d, and S3d), resulting in decomposed anomalies that are inconsistent with one another. Therefore, we are not able to draw any robust conclusions about the role of the dynamics in shaping the response to the AMO over Europe in the autumn.

During winter the circulation anomalies associated with the AMO are not clearly significant (Figs. 5b, S2b, and S3b). Cold anomalies occur over central Europe during the warm phase of the AMO but are not statistically significant and seem to be wholly controlled by the circulation anomalies (Fig. S5), as we might expect from the explained variance (Fig. 3a). However, since there is large uncertainty in the response of the large-scale circulation to the AMO, we will not focus further on the winter season. The large uncertainty highlighted here suggests that previous results linking the warm phase of the AMO to cold European temperature should be treated with some skepticism.

4. Decomposition of the AMO influence on other regions

We now apply the same method to two other regions that have been shown to be influenced by AMO variability. The same dynamical circulation analog method has been applied to monthly anomalies over Africa (30°S–45°N, 60°W–60°E) and North America (15°–90°N, 170°–50°W). The decomposed anomalies were then combined into seasonal anomalies before calculating composite differences between the warm and cold phases of the AMO, as in the previous section.

a. Sahelian rainy season

Over the Sahel region, over 90% of the annual rainfall occurs during the West African monsoon season, which peaks during August. Here we define the Sahelian rainy season as the 5-month season centered on August [i.e., June–October (JJASO)]. The AMO has been linked to multidecadal precipitation variability over the Sahel during the rainy season (e.g., Folland et al. 1986; Knight et al. 2006; Mohino et al. 2011; Ting et al. 2009; Zhang and Delworth 2006), so it is of interest to decompose the influence of the AMO into its dynamical and residual components. The SLP anomaly[2] associated with the AMO variability during the Sahelian rainy season is shown in Fig. 8. Low pressure anomalies are present across most of the tropical Atlantic (also in 20CR and HadSLP2). In particular, the significant low pressure anomaly in the tropical North Atlantic is similar to that found in previous studies (e.g., Martin and Thorncroft 2014b) and is related to an increase in the low-level West African westerly jet (Pu and Cook 2010) and associated moisture flux at around 10°N during warm AMO periods (Grist and Nicholson 2001), resulting in increased precipitation. Earlier studies found that high pressure over the tropical North Atlantic results in dry conditions over the Sahel (Hastenrath 1990). There is also a large-scale pressure gradient extending from the subtropical South Atlantic to the Sahel that is associated with cross-equatorial southerly wind anomalies, which extend onshore over the Gulf of Guinea, also resulting in increased precipitation (Hastenrath and Polzin 2011; Martin and Thorncroft 2014b).

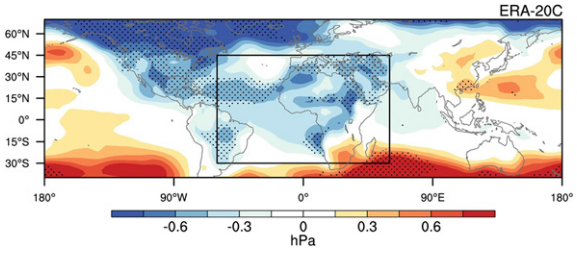

FIG. 8. Sahelian rainy season (JJASO) SLP anomaly difference between warm and cold periods of the AMO. Stippling indicates where the SLP anomaly difference is significant at the 95% level.

The differences of the full and decomposed anomaly fields between warm and cold phases of the AMO are shown in Fig. 9. The largest SAT anomalies occur over North Africa, around the Mediterranean, where warm anomalies are associated with the warm phase of the AMO over Europe (cf. Fig. 6). The warm residual SAT anomaly over northwestern Africa is likely because of advection of warmer air by the climatological northerlies in this region and is robust among all three

[2] Tests using vector wind anomalies at 925 hPa in ERA-20C, rather than SLP anomalies, yielded similar decomposed anomalies associated with the AMO.

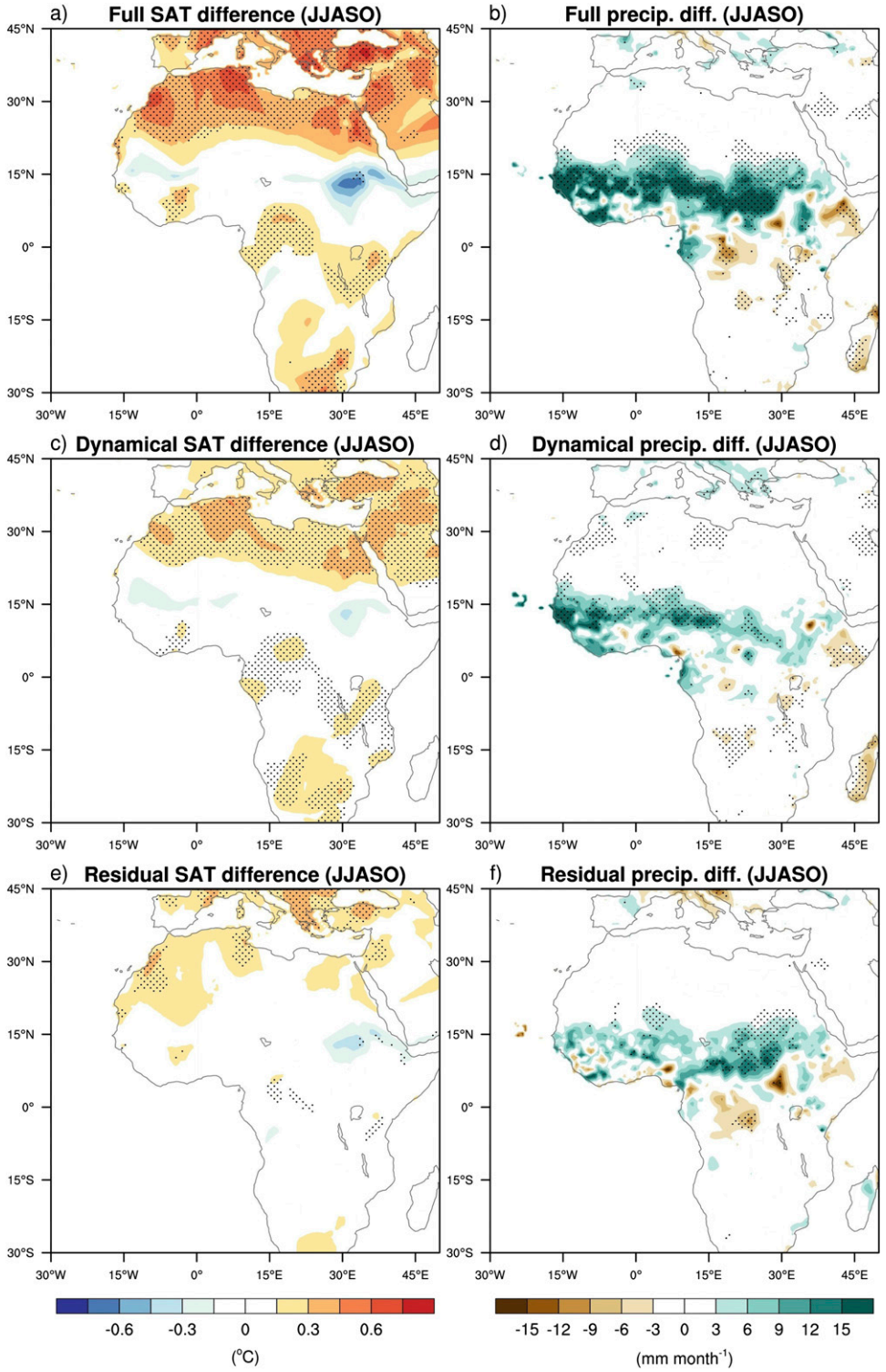

FIG. 9. Sahelian rainy season (JJASO) anomaly differences between warm and cold periods of the AMO index for the (a) full SAT anomaly, (c) dynamical SAT anomaly, (e) thermodynamical SAT anomaly, (b) full precipitation anomaly, (d) dynamical precipitation anomaly, and (f) thermodynamical precipitation anomaly. The decomposition was calculated using the ERA-20C dataset. Stippling indicates where the anomalies are significant at the 95% level.

datasets (shown in Figs. S7 and S8). As highlighted in previous studies, the clearest impact of the AMO is in precipitation over the Sahel region. In the warm phase of the AMO there is a large increase in precipitation over the Sahel during the rainy season. The decomposed fields reveal an interesting dependency on the circulation anomalies. The dynamical precipitation anomalies are positive across most of the Sahel region but particularly near the west coast, where westerly wind anomalies tend to bring moist maritime air onto the continent, which is also evident in the decompositions using 20CR and HadSLP2 (Figs. S7, S8). The residual precipitation anomalies also contribute to the positive full precipitation anomalies, reinforcing the dynamical component across the Sahel, which may be related to increased moisture flux from over the warmer SSTs by the monsoon winds. The residual component is particularly large, however, over the eastern Sahel region (Fig. 9f). In this region, there are northerly climatological winds in the lower troposphere from the eastern Mediterranean, where SSTs are significantly warmer during the warm phase of the AMO (Fig. 4). This feature is also evident in the decomposition using HadSLP2 but to a lesser extent in 20CR (Figs. S8, S9). Modeling and observational studies have previously shown that Mediterranean SSTs exhibit some control over Sahel rainfall (Gaetani et al. 2010; Park et al. 2016); however, SSTs in the tropical North Atlantic still have a more direct influence. The residual precipitation anomalies over the eastern Sahel are therefore consistent with warmer and moister air flowing south from the eastern Mediterranean toward the Sahel (Park et al. 2016; Rowell 2003).

b. *North American summer*

Many studies have highlighted the influence of the AMO on North America during summer in both models and observations (Enfield et al. 2001; Hu and Veres 2016; Knight et al. 2006; McCabe et al. 2004; Nigam et al. 2011; Ruiz-Barradas and Nigam 2005; Schubert et al. 2009; Sutton and Hodson 2005, 2007; Ting et al. 2009; Veres and Hu 2015). The circulation anomaly over North America consists of low pressure over most of the continent (Fig. 5a), and there are also low SLP anomalies over much of the tropical North Atlantic, during the warm phase of the AMO. Quite different circulation anomalies are found in 20CR and HadSLP2, with a significant low anomaly confined to the U.S. East Coast in the former, whereas there are very weak SLP anomalies across North America in the latter (Figs. S2, S3). The disparity in the dynamical response leads to significant uncertainty in the decomposed anomalies over North America, which is evident in the lower pattern correlations (Table 1).

The composite difference maps of the full and decomposed anomalies between the warm and cold phases of the AMO are shown in Fig. 10. During the warm phase of the AMO there are warm SAT anomalies over most of the continent (Fig. 10a), whereas the precipitation anomalies are mostly negative but are significantly noisier (Fig. 10b). Previous studies have highlighted the tropical North Atlantic as being particularly important over the United States, with cyclonic anomalies suppressing moisture transport into North America and resulting in warm and dry conditions during the warm phase of the AMO (Kushnir et al. 2010; Sutton and Hodson 2007). The results here are in general agreement with this picture, as dynamical SAT and precipitation anomalies are very warm and dry across much of the southeastern United States in the decomposition using the ERA-20C dataset (Figs. 10c,d). The dynamical anomalies in the 20CR and HadSLP2 decompositions agree somewhat in terms of the general characteristics of the dynamical response; however, the more pronounced cyclonic anomaly over the East Coast in 20CR explains almost the entire dynamical anomaly (Fig. S11), while in the HadSLP2 decomposition there is a significant warm residual over most of North America (Fig. S12). The residual precipitation anomalies (Fig. 10f) over the southeast of the United States, around the Gulf of Mexico, act to offset the dynamical anomalies in this region (Fig. 10d), consistent with the thermodynamic influence of increased moisture because of warm SST anomalies over the North Atlantic, resulting in relatively noisy anomalies in the full anomaly field (Fig. 10b). This offset between dynamical and thermodynamical influences is particularly stark in the decomposition using 20CR (Fig. S11). The residual SAT anomalies are positive over the western United States and across the central latitudes of North America (Fig. 10e). The AMO exhibits significant covariance with warm SST anomalies over the northeastern Pacific during summer (Fig. 4), so some of the warm residual SAT anomaly field along the west coast of North America (evident in all three datasets) could be related to anomalous warm advection from over these warm SST anomalies.

5. Discussion and summary

The constructed circulation analog method or ''dynamical adjustment'' method (Lorenz 1969) has previously been used to effectively isolate forced warming trends in midlatitudes from the considerable interannual variability (Deser et al. 2016; Smoliak et al. 2015; Wallace et al. 2012). Here we have used this technique to identify the observed impact of the AMO onto the

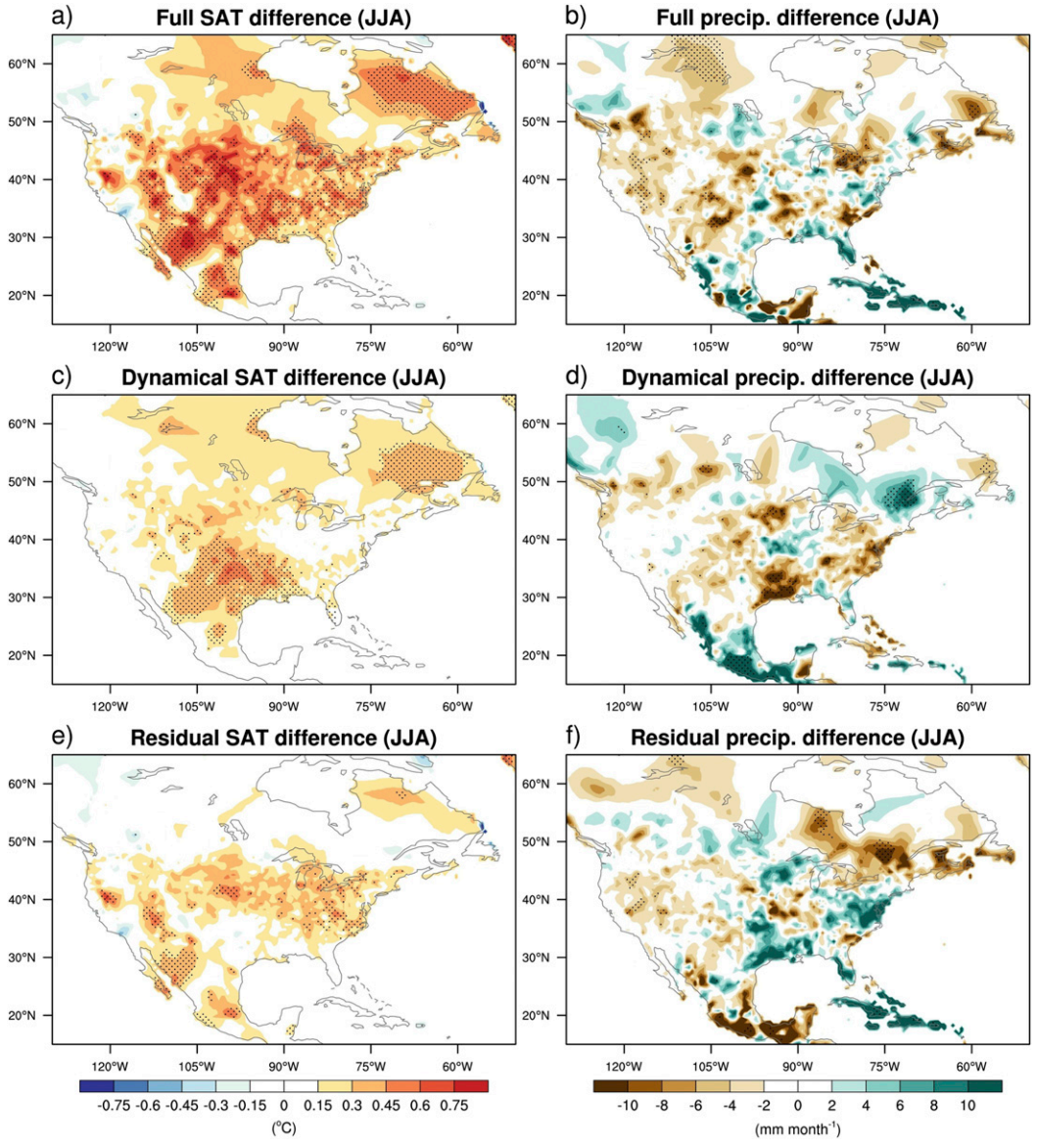

FIG. 10. Summer (JJA) anomaly differences between warm and cold periods of the AMO index for the (a) full SAT anomaly, (c) dynamical SAT anomaly, (e) thermodynamical SAT anomaly, (b) full precipitation anomaly, (d) dynamical precipitation anomaly, and (f) thermodynamical precipitation anomaly. The decomposition was calculated using the ERA-20C. Stippling indicates where the anomalies are significant at the 95% level.

atmospheric circulation and subsequently onto SAT and precipitation over adjacent continents. The method allows us to diagnose the imprint of the AMO on SAT and precipitation because of dynamical and residual influences, where in many instances the latter can be interpreted as being thermodynamical in nature.

We have focused much of our analysis on the AMO influence on European surface climate. The impact of the AMO on SAT varies greatly by season and is most significant during the summer, when continental temperatures over Europe during the positive phase of the AMO are warmer in many regions than even the North Atlantic SST [see, e.g., Fig. 4a in O'Reilly et al. (2016)]. The warm anomalies that occur during summer in the warm phase of the AMO are amplified somewhat by the circulation anomalies (e.g., Fig. 6). The significant warm residual anomaly during summer is consistent with a systematic thermodynamic influence of the warm North Atlantic, which seems to exhibit significant control on European temperatures on decadal time scales (e.g., Fig. 7). Our analysis reveals that the impact of the AMO on precipitation over Europe is generally dominated by

the dynamical anomalies. The characteristics of the influence of the AMO on the European climate during the other seasons was also considered but not presented here because the results are less robust, owing to the substantial differences between the three SLP datasets and the associated uncertainty. However, analysis of the full field decomposition demonstrates that the large-scale circulation anomalies exhibit a dominant control over SAT and precipitation anomalies, particularly during the winter season (e.g., Fig. 3). Therefore, any significant impact of the AMO over Europe during winter would be expected to be mediated by the response of the large-scale circulation to the AMO, which we found to be highly uncertain.

The influence of the circulation anomalies on the AMO impact on European climate has implications for coupled climate models and decadal prediction systems. While coupled climate models do have some multidecadal variability over Europe that is broadly consistent with the observed AMO, particularly in summer, the atmospheric response to the AMO seems to be poorly captured in all of the seasons (Kavvada et al. 2013; Ting et al. 2011); however, the nature of the observed circulation response is less clear in the autumn, winter, and spring seasons. In particular, the AMO exhibits a relatively weak impact over Europe during the summer in CMIP3/CMIP5 models compared to the observations (O'Reilly et al. 2016), which may reflect their inability to capture the extratropical atmospheric circulation response over the Euro-Atlantic sector [e.g., Fig. 8 in Kavvada et al. (2013); Fig. 9 in Ting et al. (2014)]. In winter, for example, the negative NAO-like circulation response to the AMO, which is very marginally significant (cf. Figs. 5b, S2b, and S3b), appears to be reproduced in only one of the models in the CMIP5 ensemble (Peings et al. 2016). Based on the decomposition analysis here, it is likely that the residual, thermodynamically forced anomalies in summer are more robustly simulated by climate models, after the inconsistent circulation responses are removed. Initialized decadal hindcast experiments performed with CMIP5 models have shown they are capable of capturing the persistent signal of the AMO but that predictions of multiyear SAT anomalies over Europe exhibit much lower skill (Doblas-Reyes et al. 2013; Kim et al. 2012). Analyzing the decomposed observed response to the AMO, presented in this paper, one might anticipate that decadal forecasts of SAT for the winter season would be less skillful than for the summer season, since the dynamical anomaly exhibits a much larger control over the anomalies during the winter (e.g., Fig. 3a) and a larger uncertainty. Hanlon et al. (2013) showed that, in the Met Office Decadal Climate Prediction System (DePreSys) forecasts, summer SAT anomalies were predicted with reasonable skill. It should be noted, however, that the skillful summer decadal forecasts were primarily as a result of greenhouse gas forcing. The DePreSys forecasts analyzed by Hanlon et al. (2013) exhibit no skill in predicting decadal winter SAT anomalies. This reflects the dominant control of circulation anomalies on European winter SAT and the lack of skill in predicting circulation anomalies (e.g., the NAO) over the Euro-Atlantic sector on decadal time scales (Meehl et al. 2014).

The decomposition of the AMO influence on Sahel precipitation revealed an interesting split between dynamical and residual anomalies (Fig. 9). Both dynamical and residual anomalies are substantial, with the former dominating over the western Sahel region and the latter being largest over the eastern Sahel region. Martin et al. (2014) found that the majority of CMIP5 models fail to capture the relationship between the AMO and Sahel precipitation on decadal time scales, primarily because the distribution of North Atlantic SST associated with the AMO in these models is incorrectly represented in the tropics. However, the "best" subset of the CMIP5 models is able, somewhat, to capture the North Atlantic circulation anomaly and the increase in Sahel precipitation during the warm phase of the AMO. The precipitation in these models particularly increases over the western Sahel region [see Fig. 7b of Martin et al. (2014)], consistent with the dynamical precipitation anomaly (Fig. 9d). These models, however, do not seem to capture the residual precipitation anomaly over the eastern Sahel region (Fig. 9f). The influence of the AMO on the eastern Sahel region could be related to warm SST anomalies over the Mediterranean (Gaetani et al. 2010; Park et al. 2016; Rowell 2003) during the warm phase of the AMO, but the best subset of CMIP5 models underestimates these Mediterranean SST anomalies [see Fig. 6 of Martin et al. (2014)], which could explain why the CMIP5 models fail to capture the precipitation anomalies over the eastern Sahel. It should be noted that the underestimation of the Mediterranean SST anomalies associated with the AMO is also likely to influence the ability of the CMIP5 models to capture the SAT anomalies in southern Europe in summer (i.e., Fig. 6). Decadal forecasts of Sahel precipitation exhibit reasonable skill, and the models that perform best tend to capture the magnitude and pattern of multidecadal SST variability over the North Atlantic following initialization (Gaetani and Mohino 2013; Martin and Thorncroft 2014a).

The results presented for the decomposition for the summertime impact of the AMO over North America were less clear than those over Europe and the Sahel, largely because there is some disparity between the circulation response over North America in the three

SLP datasets. There is, however, a robust warm SAT anomaly over much of the continent, particularly in the central and eastern United States, which is primarily captured in the dynamical SAT anomaly. Previous studies have shown that SAT in this region (the so-called warming hole) is well correlated with the AMO (Kumar et al. 2013). The circulation anomalies are generally associated with northerly winds in this region during the warm phase of the AMO, which has been linked to subsidence and dry conditions (Nigam et al. 2011). However, surface temperatures in the warming hole region have also been linked to the interdecadal Pacific oscillation (Meehl et al. 2012), which is not uncorrelated with the AMO, and with the impact of anthropogenic aerosol emissions over the United States (Leibensperger et al. 2012; Yu et al. 2014). There is some chance that the observed influence of the AMO on North America is affected or contaminated by these other factors rather than being purely related to multidecadal SST variability over the North Atlantic.

While the main focus of this paper has been on decomposing the influence of the AMO on continental climate, the methodology used here could prove useful for other applications. In this section, for example, we have highlighted how the dynamical decomposition could be used to reveal particular issues of model performance in response to the AMO; however, the same method could also be used to analyze other large-scale modes of SST variability (e.g., the Pacific decadal oscillation and the associated regional impacts; Newman et al. 2016). The Indian Ocean SST variability and impact on surrounding continents also likely reflects a combination of dynamical and thermodynamical components (Ummenhofer et al. 2009). Furthermore, the decomposition presented here provides a useful diagnostic with which to analyze the variability of coupled climate models and also the performance of initialized seasonal and decadal forecast systems, in which large-scale modes of SST variability are some of the most viable sources of skill.

Acknowledgments. This study was supported as part of the NERC SummerTIME project (Grant NE/M005887/1). We thank the four anonymous reviewers for their useful comments and suggestions. Insightful comments by Stephan Juricke helped to improve the manuscript.

REFERENCES

Allan, R., and T. Ansell, 2006: A new globally complete monthly historical gridded mean sea level pressure dataset (HadSLP2): 1850–2004. *J. Climate*, **19**, 5816–5842, doi:10.1175/JCLI3937.1.

Bladé, I., B. Liebmann, D. Fortuny, and G. J. van Oldenborgh, 2012: Observed and simulated impacts of the summer NAO in Europe: Implications for projected drying in the Mediterranean region. *Climate Dyn.*, **39**, 709–727, doi:10.1007/s00382-011-1195-x.

Bretherton, C. S., M. Widmann, V. P. Dymnikov, J. M. Wallace, and I. Bladé, 1999: The effective number of spatial degrees of freedom of a time-varying field. *J. Climate*, **12**, 1990–2009, doi:10.1175/1520-0442(1999)012<1990:TENOSD>2.0.CO;2.

Cattiaux, J., R. Vautard, C. Cassou, P. Yiou, V. Masson-Delmotte, and F. Codron, 2010: Winter 2010 in Europe: A cold extreme in a warming climate. *Geophys. Res. Lett.*, **37**, L20704, doi:10.1029/2010GL044613.

Compo, G. P., and Coauthors, 2011: The twentieth century reanalysis project. *Quart. J. Roy. Meteor. Soc.*, **137**, 1–28, doi:10.1002/qj.776.

Deser, C., M. A. Alexander, S.-P. Xie, and A. S. Phillips, 2010: Sea surface temperature variability: Patterns and mechanisms. *Annu. Rev. Mar. Sci.*, **2**, 115–143, doi:10.1146/annurev-marine-120408-151453.

——, L. Terray, and A. S. Phillips, 2016: Forced and internal components of winter air temperature trends over North America during the past 50 years: Mechanisms and implications. *J. Climate*, **29**, 2237–2258, doi:10.1175/JCLI-D-15-0304.1.

Doblas-Reyes, F., and Coauthors, 2013: Initialized near-term regional climate change prediction. *Nat. Commun.*, **4**, 1715, doi:10.1038/ncomms2704.

Dong, B., R. T. Sutton, T. Woollings, and K. Hodges, 2013: Variability of the North Atlantic summer storm track: Mechanisms and impacts on European climate. *Environ. Res. Lett.*, **8**, 034037, doi:10.1088/1748-9326/8/3/034037.

Enfield, D. B., A. M. Mestas-Nunez, and P. J. Trimble, 2001: The Atlantic multidecadal oscillation and its relation to rainfall and river flows in the continental U.S. *Geophys. Res. Lett.*, **28**, 2077–2080, doi:10.1029/2000GL012745.

Folland, C. K., T. Palmer, and D. Parker, 1986: Sahel rainfall and worldwide sea temperatures, 1901–85. *Nature*, **320**, 602–607, doi:10.1038/320602a0.

——, J. Knight, H. W. Linderholm, D. Fereday, S. Ineson, and J. W. Hurrell, 2009: The summer North Atlantic Oscillation: Past, present, and future. *J. Climate*, **22**, 1082–1103, doi:10.1175/2008JCLI2459.1.

Gaetani, M., and E. Mohino, 2013: Decadal prediction of the Sahelian precipitation in CMIP5 simulations. *J. Climate*, **26**, 7708–7719, doi:10.1175/JCLI-D-12-00635.1.

——, B. Fontaine, P. Roucou, and M. Baldi, 2010: Influence of the Mediterranean Sea on the West African monsoon: Intraseasonal variability in numerical simulations. *J. Geophys. Res.*, **115**, D24115, doi:10.1029/2010JD014436.

Gastineau, G., and C. Frankignoul, 2015: Influence of the North Atlantic SST variability on the atmospheric circulation during the twentieth century. *J. Climate*, **28**, 1396–1416, doi:10.1175/JCLI-D-14-00424.1.

Ghosh, R., W. A. Müller, J. Baehr, and J. Bader, 2016: Impact of observed North Atlantic multidecadal variations to European summer climate: A linear baroclinic response to surface heating. *Climate Dyn.*, **48**, 3547–3563, doi:10.1007/s00382-016-3283-4.

Grist, J. P., and S. E. Nicholson, 2001: A study of the dynamic factors influencing the rainfall variability in the West African Sahel. *J. Climate*, **14**, 1337–1359, doi:10.1175/1520-0442(2001)014<1337:ASOTDF>2.0.CO;2.

Gulev, S. K., M. Latif, N. Keenlyside, W. Park, and K. P. Koltermann, 2013: North Atlantic Ocean control on surface heat flux on multidecadal timescales. *Nature*, **499**, 464–467, doi:10.1038/nature12268.

Häkkinen, S., P. B. Rhines, and D. L. Worthen, 2011: Atmospheric blocking and Atlantic multidecadal ocean variability. *Science*, **334**, 655–659, doi:10.1126/science.1205683.

Hanlon, H. M., G. C. Hegerl, S. F. Tett, and D. M. Smith, 2013: Can a decadal forecasting system predict temperature extreme indices? *J. Climate*, **26**, 3728–3744, doi:10.1175/JCLI-D-12-00512.1.

Harris, I., P. Jones, T. Osborn, and D. Lister, 2014: Updated high-resolution grids of monthly climatic observations—The CRU TS3.10 dataset. *Int. J. Climatol.*, **34**, 623–642, doi:10.1002/joc.3711.

Hastenrath, S., 1990: Decadal-scale changes of the circulation in the tropical Atlantic sector associated with Sahel drought. *Int. J. Climatol.*, **10**, 459–472, doi:10.1002/joc.3370100504.

——, and D. Polzin, 2011: Long-term variations of circulation in the tropical Atlantic sector and Sahel rainfall. *Int. J. Climatol.*, **31**, 649–655, doi:10.1002/joc.2116.

Hu, Q., and M. C. Veres, 2016: Atmospheric responses to North Atlantic SST anomalies in idealized experiments. Part II: North American precipitation. *J. Climate*, **29**, 659–671, doi:10.1175/JCLI-D-14-00751.1.

Kållberg, P., P. Berrisford, B. Hoskins, A. Simmons, S. Lamy-Thépaut, and R. Hine, 2005: ERA-40 atlas. ECMWF ERA-40 Project Rep. 19, 199 pp.

Kavvada, A., A. Ruiz-Barradas, and S. Nigam, 2013: AMOs structure and climate footprint in observations and IPCC AR5 climate simulations. *Climate Dyn.*, **41**, 1345–1364, doi:10.1007/s00382-013-1712-1.

Kim, H.-M., P. J. Webster, and J. A. Curry, 2012: Evaluation of short-term climate change prediction in multi-model CMIP5 decadal hindcasts. *Geophys. Res. Lett.*, **39**, L10701, doi:10.1029/2012GL051644.

Knight, J. R., C. K. Folland, and A. A. Scaife, 2006: Climate impacts of the Atlantic multidecadal oscillation. *Geophys. Res. Lett.*, **33**, L17706, doi:10.1029/2006GL026242.

Kumar, S., J. Kinter III, P. A. Dirmeyer, Z. Pan, and J. Adams, 2013: Multidecadal climate variability and the warming hole in North America: Results from CMIP5 twentieth- and twenty-first-century climate simulations. *J. Climate*, **26**, 3511–3527, doi:10.1175/JCLI-D-12-00535.1.

Kushnir, Y., R. Seager, M. Ting, N. Naik, and J. Nakamura, 2010: Mechanisms of tropical Atlantic SST influence on North American precipitation variability. *J. Climate*, **23**, 5610–5628, doi:10.1175/2010JCLI3172.1.

Leibensperger, E., and Coauthors, 2012: Climatic effects of 1950–2050 changes in US anthropogenic aerosols—Part 2: Climate response. *Atmos. Chem. Phys.*, **12**, 3349–3362, doi:10.5194/acp-12-3349-2012.

Lorenz, E. N., 1969: Atmospheric predictability as revealed by naturally occurring analogues. *J. Atmos. Sci.*, **26**, 636–646, doi:10.1175/1520-0469(1969)26<636:APARBN>2.0.CO;2.

Martin, E. R., and C. D. Thorncroft, 2014a: Sahel rainfall in multimodel CMIP5 decadal hindcasts. *Geophys. Res. Lett.*, **41**, 2169–2175, doi:10.1002/2014GL059338.

——, and ——, 2014b: The impact of the AMO on the West African monsoon annual cycle. *Quart. J. Roy. Meteor. Soc.*, **140**, 31–46, doi:10.1002/qj.2107.

——, ——, and B. B. Booth, 2014: The multidecadal Atlantic SST–Sahel rainfall teleconnection in CMIP5 simulations. *J. Climate*, **27**, 784–806, doi:10.1175/JCLI-D-13-00242.1.

McCabe, G. J., M. A. Palecki, and J. L. Betancourt, 2004: Pacific and Atlantic Ocean influences on multidecadal drought frequency in the United States. *Proc. Natl. Acad. Sci. USA*, **101**, 4136–4141, doi:10.1073/pnas.0306738101.

Meehl, G. A., J. M. Arblaster, and G. Branstator, 2012: Mechanisms contributing to the warming hole and the consequent U.S. east–west differential of heat extremes. *J. Climate*, **25**, 6394–6408, doi:10.1175/JCLI-D-11-00655.1.

——, and Coauthors, 2014: Decadal climate prediction: An update from the trenches. *Bull. Amer. Meteor. Soc.*, **95**, 243–267, doi:10.1175/BAMS-D-12-00241.1.

Mohino, E., S. Janicot, and J. Bader, 2011: Sahel rainfall and decadal to multi-decadal sea surface temperature variability. *Climate Dyn.*, **37**, 419–440, doi:10.1007/s00382-010-0867-2.

Msadek, R., C. Frankignoul, and L. Z. Li, 2011: Mechanisms of the atmospheric response to North Atlantic multidecadal variability: A model study. *Climate Dyn.*, **36**, 1255–1276, doi:10.1007/s00382-010-0958-0.

Newman, M., and Coauthors, 2016: The Pacific decadal oscillation, revisited. *J. Climate*, **29**, 4399–4427, doi:10.1175/JCLI-D-15-0508.1.

Nigam, S., B. Guan, and A. Ruiz-Barradas, 2011: Key role of the Atlantic multidecadal oscillation in 20th century drought and wet periods over the Great Plains. *Geophys. Res. Lett.*, **38**, L16713, doi:10.1029/2011GL048650.

O'Reilly, C. H., M. Huber, T. Woollings, and L. Zanna, 2016: The signature of low frequency oceanic forcing in the Atlantic multidecadal oscillation. *Geophys. Res. Lett.*, **43**, 2810–2818, doi:10.1002/2016GL067925.

Park, J.-Y., J. Bader, and D. Matei, 2016: Anthropogenic Mediterranean warming essential driver for present and future Sahel rainfall. *Nat. Climate Change*, **6**, 941–945, doi:10.1038/nclimate3065.

Peings, Y., and G. Magnusdottir, 2014: Forcing of the wintertime atmospheric circulation by the multidecadal fluctuations of the North Atlantic Ocean. *Environ. Res. Lett.*, **9**, 034018, doi:10.1088/1748-9326/9/3/034018.

——, G. Simpkins, and G. Magnusdottir, 2016: Multidecadal fluctuations of the North Atlantic Ocean and feedback on the winter climate in CMIP5 control simulations. *J. Geophys. Res. Atmos.*, **121**, 2571–2592, doi:10.1002/2015JD024107.

Peña-Ortiz, C., D. Barriopedro, and R. García-Herrera, 2015: Multidecadal variability of the summer length in Europe. *J. Climate*, **28**, 5375–5388, doi:10.1175/JCLI-D-14-00429.1.

Poli, P., and Coauthors, 2013: The data assimilation system and initial performance evaluation of the ECMWF pilot reanalysis of the 20th-century assimilating surface observations only (ERA-20C). ECMWF ERA Rep. 14, 59 pp.

Pu, B., and K. H. Cook, 2010: Dynamics of the West African westerly jet. *J. Climate*, **23**, 6263–6276, doi:10.1175/2010JCLI3648.1.

Rayner, N., D. E. Parker, E. Horton, C. Folland, L. Alexander, D. Rowell, E. Kent, and A. Kaplan, 2003: Global analyses of sea surface temperature, sea ice, and night marine air temperature since the late nineteenth century. *J. Geophys. Res. Atmos.*, **108**, 4407, doi:10.1029/2002JD002670.

Rowell, D. P., 2003: The impact of Mediterranean SSTs on the Sahelian rainfall season. *J. Climate*, **16**, 849–862, doi:10.1175/1520-0442(2003)016<0849:TIOMSO>2.0.CO;2.

Ruiz-Barradas, A., and S. Nigam, 2005: Warm season rainfall variability over the U.S. Great Plains in observations, NCEP and ERA-40 reanalyses, and NCAR and NASA atmospheric model simulations. *J. Climate*, **18**, 1808–1830, doi:10.1175/JCLI3343.1.

Schubert, S., and Coauthors, 2009: A U.S. CLIVAR project to assess and compare the responses of global climate models to drought-related SST forcing patterns: Overview and results. *J. Climate*, **22**, 5251–5272, doi:10.1175/2009JCLI3060.1.

Smoliak, B. V., J. M. Wallace, M. T. Stoelinga, and T. P. Mitchell, 2010: Application of partial least squares regression to the diagnosis of year-to-year variations in Pacific Northwest snowpack and Atlantic hurricanes. *Geophys. Res. Lett.*, **37**, L03801, doi:10.1029/2009GL041478.

——, ——, P. Lin, and Q. Fu, 2015: Dynamical adjustment of the Northern Hemisphere surface air temperature field: Methodology and application to observations. *J. Climate*, **28**, 1613–1629, doi:10.1175/JCLI-D-14-00111.1.

Sutton, R. T., and D. L. Hodson, 2005: Atlantic Ocean forcing of North American and European summer climate. *Science*, **309**, 115–118, doi:10.1126/science.1109496.

——, and ——, 2007: Climate response to basin-scale warming and cooling of the North Atlantic Ocean. *J. Climate*, **20**, 891–907, doi:10.1175/JCLI4038.1.

——, and B. Dong, 2012: Atlantic Ocean influence on a shift in European climate in the 1990s. *Nat. Geosci.*, **5**, 788–792, doi:10.1038/ngeo1595.

Ting, M., Y. Kushnir, R. Seager, and C. Li, 2009: Forced and internal twentieth-century SST trends in the North Atlantic. *J. Climate*, **22**, 1469–1481, doi:10.1175/2008JCLI2561.1.

——, ——, ——, and ——, 2011: Robust features of Atlantic multidecadal variability and its climate impacts. *Geophys. Res. Lett.*, **38**, L17705, doi:10.1029/2011GL048712.

——, ——, and C. Li, 2014: North Atlantic multidecadal SST oscillation: External forcing versus internal variability. *J. Mar. Syst.*, **133**, 27–38, doi:10.1016/j.jmarsys.2013.07.006.

Ummenhofer, C. C., A. Sen Gupta, M. H. England, and C. J. Reason, 2009: Contributions of Indian Ocean sea surface temperatures to enhanced East African rainfall. *J. Climate*, **22**, 993–1013, doi:10.1175/2008JCLI2493.1.

Van den Dool, H., 1994: Searching for analogues, how long must we wait? *Tellus*, **46A**, 314–324, doi:10.3402/tellusa.v46i3.15481.

——, J. Huang, and Y. Fan, 2003: Performance and analysis of the constructed analogue method applied to US soil moisture over 1981–2001. *J. Geophys. Res.*, **108**, 8617, doi:10.1029/2002JD003114.

Veres, M., and Q. Hu, 2015: Atmospheric responses to North Atlantic SST anomalies in idealized experiments. Part I: Northern Hemispheric circulation. *J. Climate*, **28**, 6204–6220, doi:10.1175/JCLI-D-14-00413.1.

von Storch, H., and F. W. Zwiers, 2002: *Statistical Analysis in Climate Research*. Academic Press, 496 pp.

Wallace, J. M., Q. Fu, B. V. Smoliak, P. Lin, and C. M. Johanson, 2012: Simulated versus observed patterns of warming over the extratropical Northern Hemisphere continents during the cold season. *Proc. Natl. Acad. Sci. USA*, **109**, 14 337–14 342, doi:10.1073/pnas.1204875109.

Yamamoto, A., and J. B. Palter, 2016: The absence of an Atlantic imprint on the multidecadal variability of wintertime European temperature. *Nat. Commun.*, **7**, 10930, doi:10.1038/ncomms10930.

Yu, S., K. Alapaty, R. Mathur, J. Pleim, Y. Zhang, C. Nolte, B. Eder, K. Foley, and T. Nagashima, 2014: Attribution of the United States "warming hole": Aerosol indirect effect and precipitable water vapor. *Sci. Rep.*, **4**, 6929, doi:10.1038/srep06929.

Zhang, R., and T. L. Delworth, 2006: Impact of Atlantic multidecadal oscillations on India/Sahel rainfall and Atlantic hurricanes. *Geophys. Res. Lett.*, **33**, L17712, doi:10.1029/2006GL026267.